Spin-Torque Microwave Detectors

Oleksandr V. Prokopenko[1], Ilya N. Krivorotov[2], Thomas J. Meitzler[3],

Elena Bankowski[3], Vasil S. Tiberkevich[4] and Andrei N. Slavin[4]

[1] Faculty of Radiophysics, Taras Shevchenko National University of Kyiv
Kyiv, 01601, Ukraine, ovp@univ.kiev.ua

[2] Department of Physics and Astronomy, University of California
Irvine, CA 92697, USA, ikrivoro@uci.edu

[3] U.S. Army TARDEC, Warren, MI 48397, USA,
elena.n.bankowski.civ@.mail.mil, thomas.j.meitzler.civ@.mail.mil

[4] Department of Physics, Oakland University
Rochester, MI 48309, USA, tyberkev@oakland.edu, slavin@oakland.edu

Abstract. It is known that the spin-transfer torque (STT) effect provides a new method of manipulation of magnetization in nano-scale objects. According to the STT effect bias DC current traversing magnetic multilayers can transfer angular magnetic moments from one layer to another, which can give rise to the microwave dynamics of magnetization in the layer. However, it is clear that an inverse effect is also possible. This inverse effect leads to the so-called spin-torque diode effect, first originally observed experimentally in 2005. The spin torque diode effect is a rectification effect of the input microwave current in a magnetoresistive junction. In this case, the resonance oscillations of the junction resistance can mix with the oscillations of the input microwave current and produce a large enough output DC voltage across the junction. The devices, which utilize this effect, are called the spin-torque microwave detectors (STMD). In this chapter we review the general properties of STMDs and consider the performance of a STMD in two different dynamic regimes of detector operation: in the well-known traditional in-plane regime of STMD operation and in the recently discovered novel out-of-plane regime of STMD operation. We analyze the performance of a STMD and consider the typical applications for such detectors in both regimes.

Report Documentation Page

Form Approved
OMB No. 0704-0188

1. REPORT DATE	2. REPORT TYPE	3. DATES COVERED
06 FEB 2012	**Technical Report**	**06-02-2012 to 06-02-2012**

4. TITLE AND SUBTITLE
SPIN-TORQUE MICROWAVE DETECTORS

5a. CONTRACT NUMBER
5b. GRANT NUMBER
5c. PROGRAM ELEMENT NUMBER

6. AUTHOR(S)
Elena Bankowski; Vasil Tiberkevich; Thomas Meitzler; Andrei Slavin; Oleksandr Prokoponke

5d. PROJECT NUMBER
5e. TASK NUMBER
5f. WORK UNIT NUMBER

7. PERFORMING ORGANIZATION NAME(S) AND ADDRESS(ES)
Oakland University,Department of Physics,Rochester,MI,48309

8. PERFORMING ORGANIZATION REPORT NUMBER
; #22564

9. SPONSORING/MONITORING AGENCY NAME(S) AND ADDRESS(ES)
U.S. Army TARDEC, 6501 E.11 Mile Rd, Warren, MI, 48397-5000

10. SPONSOR/MONITOR'S ACRONYM(S)
TARDEC

11. SPONSOR/MONITOR'S REPORT NUMBER(S)
#22564

12. DISTRIBUTION/AVAILABILITY STATEMENT
Approved for public release; distribution unlimited

13. SUPPLEMENTARY NOTES

14. ABSTRACT

It is known that the spin-transfer torque (STT) effect provides a new method of manipulation of magnetization in nano-scale objects. According to the STT effect bias DC current traversing magnetic multilayers can transfer angular magnetic moments from one layer to another, which can give rise to the micro-wave dynamics of magnetization in the layer. However, it is clear that an inverse effect is also possible. This inverse effect leads to the so-called spin-torque diode effect, first originally observed experimentally in 2005. The spin torque diode effect is a rectification effect of the input microwave current in a magnetoresistive junction. In this case, the resonance oscillations of the junction resistance can mix with the oscillations of the input microwave current and produce a large enough output DC voltage across the junction. The devices, which utilize this effect, are called the spin-torque microwave detectors (STMD). In this chapter we review the general properties of STMDs and consider the performance of a STMD in two dif-ferent dynamic regimes of detector operation: in the well-known traditional in-plane regime of STMD operation and in the recently discovered novel out-of-plane regime of STMD operation. We analyze the performance of a STMD and consider the typical applications for such detectors in both regimes.

15. SUBJECT TERMS

16. SECURITY CLASSIFICATION OF:			17. LIMITATION OF ABSTRACT	18. NUMBER OF PAGES	19a. NAME OF RESPONSIBLE PERSON
a. REPORT	b. ABSTRACT	c. THIS PAGE			
unclassified	**unclassified**	**unclassified**	**Same as Report (SAR)**	**22**	

1 Introduction

The spin-transfer-torque (STT) effect in magnetic multilayers was theoretically predicted in [1, 2] and experimentally observed in [3–13]. It provides a new method of manipulation of the magnetization direction in nano-magnetic systems [14]: magnetization switching [3, 4], generation of microwave oscillations under the action of a dc electric current [5–11] and the spin torque diode effect [12–13], which can then be used for the development of practical microwave detectors, so called spin-torque microwave detectors (STMD), and also for quantitatively measuring STT [15, 16].

The spin torque diode effect is a quadratic rectification effect of the input microwave current $I_{RF}(t)$ in a magnetoresistive junction, which is commonly observed in traditional regime of operation of a STMD, when the frequency f_s of the current $I_{RF}(t) = I_{RF}\sin(2\pi f_s t)$ is close to the ferromagnetic resonance (FMR) frequency f_0 of the junction. In this case the induced resonance oscillations of the junction resistance $R(t)$ can mix with the oscillations of the input microwave current $I_{RF}(t)$ and produce a sufficiently large output DC voltage $U_{DC} = \langle I_{RF}(t)R(t)\rangle$ across the junction (here $\langle ...\rangle$ denotes averaging over the period of oscillations $1/f_0$).

In the traditional in-plane (IP) regime of operation of a STMD [12, 13, 17] the STT excites a *small-angle in-plane* magnetization precession about the equilibrium direction of magnetization in the "free" layer (FL) of a magnetic tunnel junction (MTJ) (see the red dashed curve in Fig. 1). Below we shall refer to this regime of STMD operation as the IP-regime. Using analytical theory we

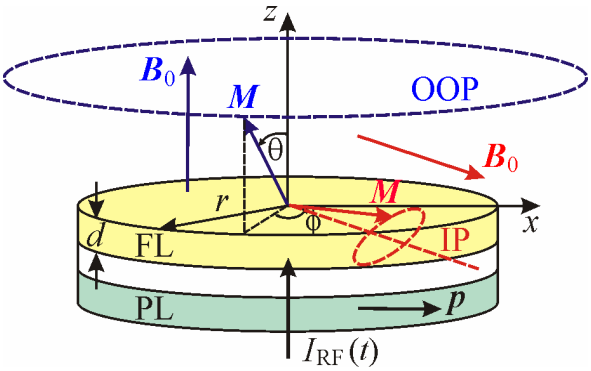

Fig. 1. The model of a STMD: circular nano-pillar of radius r consists of the "free" magnetic layer (FL) of thickness d and the "pinned" magnetic layer (PL). Under the action of microwave current $I_{RF}(t)$, the magnetization vector $\boldsymbol{M}$ (shown by a blue or red arrow) is precessing along small-angle in-plane (red dashed curve, IP-regime) or large-angle out-of-plane (blue dashed curve, OOP-regime) trajectory about the direction of the bias magnetic field $\boldsymbol{B}_0$ (shown by a red or blue arrow), $\boldsymbol{p} = \boldsymbol{x}$ is the unit vector in the direction of the magnetization of the PL, $\boldsymbol{x}$ is the unit vectors of x-axis.

show that the performance of a passive STMD in the IP-regime is limited by thermal noise. We also show how to calculate the optimal parameters of a STMD operating in this regime. We believe, that the formalism developed can be used for optimization of noise-handling properties for construction of a practical STMD.

In contrast to the well-known IP-regime of STMD operation, in this paper we also consider a different regime of operation of an STMD, based on the excitation of *large-angle out-of-plane* (OOP) magnetization precession under the action of an input microwave current $I_{RF}(t)$ (see the blue dashed curve in Fig. 1). Using analytical and numerical calculations, we show that all the major STMD characteristics in the OOP-regime qualitatively differ from the ones in the traditional IP-regime. In particular, excitations in the OOP-regime do not have a resonance character and exist in a wide range of driving frequencies. Also, the output DC voltage of an STMD in the OOP regime is nearly independent of the input microwave power, provided it exceeds a certain threshold value. We believe that these properties of an STMD in the OOP-regime will be useful for the development of nano-sized threshold detectors with a large output DC voltage, spectrum analyzers, and also for the applications in microwave energy harvesting in the low-frequency region of the microwave band.

2 Basic physics of STT and TMR

The operation of a STMD based on the MTJ is based on two related phenomena: tunneling magnetoresistance (TMR) and the above mentioned STT.

The phenomenon of TMR exists because of the dependence of the resistance $R(\beta)$ of a MTJ on the angle β between magnetizations of the two ("free" and "pinned") magnetic layers of the junction. Here we shall consider only symmetric unbiased junctions, for which $R(\beta)$ can be written as [17]

$$R(\beta) = \frac{R_\perp}{1 + P^2 \cos\beta}, \tag{1}$$

where $R_\perp$ is the junction's resistance in the perpendicular ($\beta = \pi/2$) magnetic state and P is the dimensionless spin-polarization efficiency. Conventional parallel (R_P) and antiparallel (R_{AP}) resistances are connected with $R_\perp$ and P by

$$R_P = \frac{R_\perp}{1+P^2}, \quad R_{AP} = \frac{R_\perp}{1-P^2}, \tag{2}$$

whereas conventional TMR ratio can be caculated as

Fix TMR to not italicize $\mathrm{T}MR = \frac{R_{AP} - R_P}{R_P} = \frac{2P^2}{1-P^2}.$ (3)

Typical values of P are about $0.5 - 0.7$, whereas $R_\perp$ can be estimated as

$$R_{\perp} = \frac{RA}{S}\,, \tag{4}$$

where $RA \sim 1-10\,\Omega\cdot\mu\mathrm{m}^2$ is the resistance-area product of the MTJ and S is its area. For typical sub-micron sizes of the junction, $R_{\perp}$ is much higher than the characteristic impedance $Z_{TL} = 50\,\Omega$ of standard microwave transmission lines.

The phenomenon of STT is the complementary effect to TMR. The STT phenomenon is the appearance of an additional torque which acts on the magnetizations of junctions' layers, when an electric current $I(t)$ passes through the junction. We shall consider the case when the magnetization in one of the layers ("pinned" magnetic layer) is completely pinned and shall consider magnetization dynamics only in another ("free") magnetic layer (FL). The additional STT that acts on the magnetization $\mathbf{M}$ of this layer can be written as

$$\left(\frac{d\mathbf{M}}{dt}\right)_{STT} = \frac{\sigma(\beta)I(t)}{M_s}[\mathbf{M}\times[\mathbf{M}\times\mathbf{p}]]\,, \tag{5}$$

where $M_s = |\mathbf{M}|$ is the saturation magnetization of the FL, $\mathbf{p}$ is the unit vector in the direction of the magnetization of the PL, and $\sigma(\beta)$ is the current-torque proportionality coefficient that is equal to

$$\sigma(\beta) = \frac{\sigma_{\perp}}{1+P^2\cos\beta}\,,\quad \sigma_{\perp} = \frac{\gamma\hbar}{2e}\frac{P}{M_s V}\,. \tag{6}$$

Here $\gamma \approx 2\pi\cdot 28\,\mathrm{GHz/T}$ is the modulus of the gyromagnetic ratio, $\hbar$ is the reduced Planck constant, e is the modulus of the electron charge, and $V = Sd$ is the volume of the FL (d is its thickness).

3 Small-angle in-plane dynamical regime of STMD operation

In the traditional regime of operation of a STMD (based on the above mentioned spin torque diode effect) the STT excites a small-angle in-plane magnetization precession about the equilibrium direction of the magnetization in the "free" magnetic layer (FL) of a junction (the trajectory of magnetization precession is shown by a red dashed curve in Fig. 1). The precessional motion of magnetization in the IP-regime determines the following typical properties of a traditional STMD [12–13, 17]:

(a) The STMD operates as a frequency-selective microwave detector with a resonance frequency that is close to the frequency of the ferromagnetic resonance (FMR) $\omega_0 = 2\pi f_0$ of the FL;

(b) The frequency operation range of the detector has an order of the FMR linewidth Γ;

(c) The output DC voltage U_{DC} of the STMD is proportional to the input microwave power $P_{RF} = I_{RF}^2 R_0/2$ (R_0 is the equilibrium MTJ resistance), so the spin-torque diode operates as a resonance-type, quadratic microwave detector:

$$U_{DC} = \varepsilon_{res} P_{RF} \frac{\Gamma^2}{\Gamma^2 + (\omega_s - \omega_0)^2}, \quad (7)$$

where

$$\varepsilon_{res} = \frac{\gamma\hbar}{4e} \frac{P^3}{M_s V \Gamma} Q(\beta_0) \quad (8)$$

is the resonance (at $\omega_s = \omega_0$) diode volt-watt sensitivity (see [17]). Here $Q(\beta_0)$ is the geometrical factor that depends on the angle β_0 between the directions of the equilibrium magnetization in FL and PL of the MTJ. For an in-plane magnetized MTJ:

$$Q(\beta_0) = \frac{\sin^2(\beta_0)}{\left(1 + P^2 \cos\beta_0\right)^2}; \quad (9)$$

(d) the diode resonance sensitivity ε_{res} strongly depends on the angle β between magnetization directions of the FL and PL – see Eq. (9).

The resonance sensitivity of traditional STMD $\varepsilon_{res} = U_{DC} / P_{RF}$ is predicted to be approximately $\varepsilon_{res} \sim 10^4 \text{ V/W}$ (see [17]), while the best achieved experimental result to date is $\varepsilon_{res} \approx 300 \text{ V/W}$ [13].

3.1 Analytical theory of noise properties of a STMD in IP-regime

It is known that the operation and the minimum detectable power of all types of microwave detectors are limited by noise (in particular, by the low-frequency Johnson-Nyquist noise in the case of unbiased Schottky diodes [18]), and, therefore, it is important to understand the noise-handling properties of the novel STMD based on MTJ – this is the main aim of this part of the paper.

Below we present a theoretical analysis of the noise properties of a passive resonance-type STMD (no DC bias current) using the STMD model developed in [17] with additional terms describing influence of thermal fluctuations. The results presented below are expanded and are complementary to the results presented in [19].

During the theoretical analysis we use the following assumptions:

(a) we assume that the lateral sizes of STMD FL are sufficiently small, so the internal magnetization dynamics can be described in the macrospin approximation;

(b) the PL is assumed to be truly "pinned", i.e. we neglect any possible fluctuations or oscillations of magnetization in this layer;

(c) we consider unbiased STMD, i.e. the current $I(t)$ flowing through STMD has only microwave component $I_{RF}(t)$, $I(t) = I_{RF}(t)$;

(d) amplitude of the detected current I_{RF}, as well as the temperature of the

system T, is assumed to be sufficiently small to provide a linear response of the magnetization to the current and thermal fluctuations. This also means, that in all expressions we shall keep only the lowest-order (of the current amplitude and temperature) non-zero terms;

(e) we shall consider only the case of a low-damping STMD $f_0 >> \Gamma / 2\pi$, in which case one can drop non-resonant terms in the detected output voltage U_{DC};

(f) we also assume that the frequency interval of the detection Δf (inversely proportional to the measurement time) is much smaller than the FMR linewidth $\Gamma / 2\pi$ in the FL, $\Delta f << \Gamma / 2\pi$. This means that we are interested only in the zero-frequency limit of the noise spectral density of the output voltage;

(g) at last, we assume that the noise temperature T for all considered below noise sources is the same.

There are several possible sources of noise in STMD. Moreover, since the operation of the STMD is necessary nonlinear, the noise is, in general, not additive and can depend on the amplitude and frequency of the detected signal. Among all possible noise sources we shall consider only the following:

(a) *Low-frequency Johnson-Nyquist* (JN) *noise*, i.e. low-frequency voltage fluctuations $U_N(t)$ associated with the equilibrium electrical resistance of the STMD R_0. This type of the noise is additive and is independent of the magnetization dynamics.

(b) *High-frequency Johnson-Nyquist noise*. In contrast with the low-frequency components, microwave part of the JN noise does not contribute to the output detected signal directly. A microwave noise current $I_N(t)$, however, can induce additional fluctuations of the magnetization direction in the FL and, respectively, fluctuations of the electrical resistance of the STMD. Being mixed with the detected current $I_{RF}(t)$, these resistance fluctuations will create non-additive low-frequency noise in the output voltage U_{DC}.

(c) *Magnetic noise* (MN), which is caused by the thermal fluctuations of the magnetization direction in the MTJ FL, is modeled by the action of a random white Gaussian magnetic field $\mathbf{B}_N(t)$, leads to the fluctuations of the electric resistance of the STMD. It is transformed into low-frequency noise after mixing with the driving current $I_{RF}(t)$.

The other noise sources, such as shot noise and flicker noise, might be important for STMDs biased by a DC current.

To calculate the noise spectrum in a STMD we shall, first, calculate the linear response of the magnetization of the FL to arbitrary microwave currents and magnetic fields. Then we shall calculate corresponding variations of the electrical resistance of the STMD, i.e. calculate the electrical response of STMD to currents and fields. After that, using a simplified electrical scheme of STMD, we shall calculate the STMD noise spectrum.

Dynamics of the magnetization $\mathbf{M}$ of the FL under the action of microwave

current $I(t)$ and magnetic field $\mathbf{B}(t)$ are described by the Landau-Lifshits-Gilbert-Slonczewski equation:

$$\frac{d\mathbf{M}}{dt} = \gamma[\mathbf{B}_{eff}(\mathbf{M}) \times \mathbf{M}] + \frac{\alpha}{M_s}\left[\mathbf{M} \times \frac{d\mathbf{M}}{dt}\right] + \\ + \frac{\sigma(\beta) I(t)}{M_s}[\mathbf{M} \times [\mathbf{M} \times \mathbf{p}]] + \gamma[\mathbf{B}(t) \times \mathbf{M}]. \quad (10)$$

Here $\mathbf{B}_{eff}(\mathbf{M})$ is the effective magnetic field, which includes the external bias magnetic field $\mathbf{B}_0$ and the demagnetization field, α is the Gilbert damping constant. The first term in the right-hand side of Eq. (10) describes conservative magnetization precession, the second term describes magnetic dissipation, and the last two terms describe excitation of the magnetization precession by the microwave current $I(t)$ and magnetic field $\mathbf{B}(t)$, respectively.

To find the linear response of the magnetization, we represent $\mathbf{M}$ in the form

$$\mathbf{M}(t) = (\mathbf{m}_0 + \mathbf{m}(t))M_s, \quad (11)$$

where $\mathbf{m}_0$ is the unit vector in the direction of the equilibrium orientation of the magnetization vector and $\mathbf{m}(t)$ is the dimensionless amplitude of small magnetization precession. In the considered linear regime the vectors $\mathbf{m}_0$ and $\mathbf{m}(t)$ are orthogonal to each other. Substituting Eq. (11) into Eq. (10) and keeping only linear terms in $\mathbf{m}$, $I(t)$, and $\mathbf{B}(t)$ yields the linear equation for $\mathbf{m}(t)$:

$$\frac{d\mathbf{m}}{dt} = -i\hat{\mathbf{L}} \cdot \mathbf{m} + \alpha\left[\mathbf{m}_0 \times \frac{d\mathbf{m}}{dt}\right] + \sigma_0 I(t)[\mathbf{m}_0 \times [\mathbf{m}_0 \times \mathbf{p}]] + \gamma[\mathbf{B}(t) \times \mathbf{m}_0], \quad (12)$$

(operator above L is not evident in WORD) where $\sigma_0 = \sigma(\beta_0)$ and the linear operator $\hat{\mathbf{L}}$ is determined by the linearization of the first conservative term in the right hand side of Eq. (10). It is clear (and can be easily proven rigorously) that the vector $\mathbf{m}_0$ is the eigenvector of the operator $\hat{\mathbf{L}}$ corresponding to the eigenvalue 0. The two other eigenvectors are complex conjugaes (i.e., $\boldsymbol{\mu}$ and $\boldsymbol{\mu}^*$) and correspond to opposite eigenvalues (i.e., $\omega_0 > 0$ and $-\omega_0 < 0$). These eigenvectors are orthogonal to $\mathbf{m}_0$ and, respectively, span the vector space of small magnetization oscillations $\mathbf{m}(t)$. Taking into account that $\mathbf{m}(t)$ is a real-valued vector, we can represent it as

$$\mathbf{m}(t) = \boldsymbol{\mu} c(t) + \text{c.c.}, \quad (13)$$

where $c(t)$ is the complex amplitude of precession and c.c. denotes complex-

conjugated part.

Substituting Eq. (13) into Eq. (12) and taking scalar product of both sides of this equation with $[\mathbf{m}_0 \times \boldsymbol{\mu}^*]$ gives a simple equation for the rate of change of $c(t)$:

$$\frac{dc}{dt} = -i\omega_0 c - \Gamma c + \sigma_0 \tilde{q} I(t) + \gamma \tilde{\mathbf{u}} \cdot \mathbf{B}(t). \tag{14}$$

Here Γ is the damping rate of magnetization precession,

$$\Gamma = i\alpha\omega_0 \frac{|\boldsymbol{\mu}|^2}{(\boldsymbol{\mu}, \mathbf{m}_0, \boldsymbol{\mu}^*)}, \tag{15}$$

and dimensionless current $\tilde{q}$ and field $\tilde{\mathbf{u}}$ "susceptibilities" are equal to

$$\tilde{q} = -\frac{(\mathbf{p}, \mathbf{m}_0, \boldsymbol{\mu}^*)}{(\boldsymbol{\mu}, \mathbf{m}_0, \boldsymbol{\mu}^*)}, \quad \tilde{\mathbf{u}} = -\frac{\boldsymbol{\mu}^*}{(\boldsymbol{\mu}, \mathbf{m}_0, \boldsymbol{\mu}^*)}. \tag{16}$$

Here notation $(\mathbf{v}_1, \mathbf{v}_2, \mathbf{v}_3)$ denotes scalar triple product, please check this notation for scaler of vector product) $(\mathbf{v}_1, \mathbf{v}_2, \mathbf{v}_3) = \mathbf{v}_1 \cdot [\mathbf{v}_2 \times \mathbf{v}_3]$. Note that the "tilded" susceptibilities $\tilde{q}$ and $\tilde{\mathbf{m}}$ depend on the normalization of the eigenvector $\boldsymbol{\mu}$ and, respectively, do not have a physical meaning.

Equation (14) can be easily solved in the frequency representation:

$$c_\omega = \frac{\sigma_0 \tilde{q}}{\Gamma_\omega} I_\omega + \frac{\gamma \tilde{\mathbf{u}}}{\Gamma_\omega} \cdot \mathbf{B}_\omega, \tag{17}$$

where

$$\Gamma_\omega = \Gamma - i(\omega - \omega_0). \tag{18}$$

Finally, the magnetization response $\mathbf{m}$ in the frequency representation is given by

$$\mathbf{m}_\omega = \sigma_0 \left(\frac{\tilde{q}\boldsymbol{\mu}}{\Gamma_\omega} + \frac{\tilde{q}^* \boldsymbol{\mu}^*}{\Gamma^*_{-\omega}} \right) I_\omega + \gamma \left(\frac{\boldsymbol{\mu}\tilde{\mathbf{u}}}{\Gamma_\omega} + \frac{\boldsymbol{\mu}^* \tilde{\mathbf{u}}^*}{\Gamma^*_{-\omega}} \right) \cdot \mathbf{B}_\omega, \tag{19}$$

where we took into account that both $I(t)$ and $\mathbf{B}(t)$ are real-valued and, respectively, $I_\omega = I^*_{-\omega}$ and $\mathbf{B}_\omega = \mathbf{B}^*_{-\omega}$.

The expressions derived above give the complete information about the magnetization response on an arbitrary microwave current $I(t)$ and magnetic field $\mathbf{B}(t)$ provided that equilibrium magnetization direction $\mathbf{m}_0$, vector structure of the precession mode $\boldsymbol{\mu}$, PL magnetization orientation $\mathbf{p}$, and FMR frequency ω_0 are known. Calculation of all these parameters can be easily done in each particular case.

From the "electrical" point of view, STMD is a resistance $R(\beta)$ that depends on the angle $\beta = \arccos(\mathbf{M} \cdot \mathbf{p} / M_s)$ between magnetizations of the "free" and

"pinned" layers. Since the magnetization of the FL oscillates, the resistance $R(\beta)$ changes in time and can be written as

$$R = R_0 + \delta R(t), \qquad \delta R(t) = R_0 \rho \delta\beta(t), \tag{20}$$

where $R_0 = R(\beta_0)$ is the equilibrium STMD resistance, $\beta_0 = \arccos(\mathbf{m}_0 \cdot \mathbf{p})$ is the equilibrium angle, and

$$\rho = \frac{1}{R_0}\left(\frac{dR}{d\beta}\right)_{\beta=\beta_0} = \frac{P^2 \sin\beta_0}{1 + P^2 \cos\beta_0} \tag{21}$$

is the dimensionless slope of the angular dependence of the resistance $R(\beta)$ at the equilibrium and angular variations $\delta\beta$ can be written as

$$\delta\beta(t) = -\frac{\mathbf{m}(t) \cdot \mathbf{p}}{\sin\beta_0} . \tag{22}$$

The output signal of a STMD consists of the low-frequency components of the voltage drop across the STMD. We assume that the high-frequency components are completely filtered out by an external circuit and that there is no low-frequency current (electrical circuit of STMD is open at low frequencies). Then, the output voltage $U_{out}(t)$ can be written as

$$U_{out}(t) = \left[U_{JN}(t) + \delta R(t) I(t)\right]_{\omega \to 0} , \tag{23}$$

where $U_{JN}(t)$ is the JN voltage noise, $I(t)$ is the microwave current through the STMD, and notation $[\ldots]_{\omega \to 0}$ symbolically denotes filtering of low-frequency components. The term $R_0 I(t)$ does not give any contribution to the low-frequency signal and has been omitted.

The current $I(t)$ consists of the input signal current $I_{RF}(t) = I_{RF} \sin(\omega_s t)$, where ω_s is the signal frequency, and noise current $I_N(t) = U_N(t) / R_0$ created by the microwave components of the JN voltage noise. The resistance fluctuations $\delta R(t)$ are created by the current $I(t)$ and thermal noise magnetic field $\mathbf{B}_N(t)$.

The detected voltage U_{DC} is obtained from Eq. (23) by taking into account only the signal components:

$$U_{DC} = \mathrm{Re}\left(\frac{\rho q}{2} \frac{R_0 \sigma_0}{\Gamma_{\omega_s}}\right) I_{RF}^2 , \tag{24}$$

where we have dropped the non-resonant term (proportional to $1/\Gamma_{-\omega_s}$), which can be done for low-damping STMD ($\omega_0 >> \Gamma$); $q = -(\boldsymbol{\mu} \cdot \mathbf{p})\tilde{q} / \sin\beta_0$.

To calculate the spectrum of the low-frequency noise, one has to take into account that the JN voltage $U_{JN}(t)$ and thermal magnetic field $\mathbf{B}_N(t)$ are independent random white Gaussian processes with constant spectral densities (spectral density $S_f(\omega)$ of a stationary random process), $f(t)$ is defined by

$\left\langle f_\omega f^*_{\omega'} \right\rangle = 2\pi\delta(\omega-\omega')S_f(\omega)$):

$$S(U_N) = S(I_N)R_0^2 = 2k_BTR_0\ ,\quad S(B_N) = \frac{2\alpha k_BT}{\gamma M_sV}\ , \tag{25}$$

where k_B is the Boltzmann constant. The spectral density $S(B_N)$ is the correlator of the same vector components of $\mathbf{B}_N(t)$; different components of $\mathbf{B}_N$ are independent.

Calculation of the output voltage noise spectrum $S_{out}(\Omega)$, where Ω is the frequency of the output voltage fluctuations, from Eq. (23) gives

$$S_{out}(\Omega) = S^{(1)}_{out}(\Omega) + S^{(2)}_{out}(\Omega) + S^{(3)}_{out}(\Omega)\ , \tag{26}$$

where

$$S^{(1)}_{out}(\Omega) = S(U_N)\,, \tag{27}$$

$$S^{(2)}_{out}(\Omega) = \frac{1}{4}S(U_N)\sigma_0^2\rho^2I_{RF}^2\left[\left|\frac{q}{\Gamma_{\omega_s}} + \frac{q^*}{\Gamma^*_{\omega_s-\Omega}}\right|^2 + \left|\frac{q}{\Gamma_{\omega_s}} + \frac{q^*}{\Gamma^*_{\omega_s+\Omega}}\right|^2\right], \tag{28}$$

$$S^{(3)}_{out}(\Omega) = \frac{1}{4}S(B_N)R_0^2\gamma^2\rho^2u^2I_{RF}^2\left[|\Gamma_{\omega_s-\Omega}|^{-2} + |\Gamma_{\omega_s+\Omega}|^{-2}\right]. \tag{29}$$

The three terms $S^{(1,2,3)}_{out}(\Omega)$ are caused, respectively, by (i) low-frequency components of the JN noise, (ii) high-frequency components of the JN noise and related fluctuations of the MTJ resistance, and (iii) fluctuations of the MTJ resistance due to thermal magnetic field.

As one can see from Eqs. (26) – (29), the frequency dependence of the detector noise is completely determined by the frequency dependence of the damping factor Γ_ω (see Eq. (18)). In the following we assume, for simplicity, that the signal frequency ω_s exactly coincides with the FMR frequency ω_0 and that the frequency interval of detection $\Delta f \approx \Omega/2\pi$ (inversely proportional to the measurement time) is much smaller than the FMR linewidth $\Gamma/2\pi$.

In such a resonant case Eq. (24) becomes

$$U_{DC} = \left(\frac{\rho q_r}{2}\frac{R_0\sigma_0}{\Gamma}\right)I_{RF}^2 = \rho q_r\frac{\sigma_0}{\Gamma}P_{RF}\,, \tag{30}$$

where $q_r = \mathrm{Re}(q)$.

The noise spectrum, S_{out}, in this case can be written in a very simple form

$$S_{out} = \left(1 + \frac{U_{DC}}{U_{IM}} + \frac{U_{DC}}{U_{MN}}\right)S(U_N)\,, \tag{31}$$

where

$$U_{IM} = \frac{R_0 \Gamma}{4\rho q_r \sigma_0}, \quad U_{MN} = \frac{q_r \sigma_0 M_s V \Gamma}{\alpha \rho u^2 \gamma}. \tag{32}$$

Finally, root mean square fluctuations of the output voltage ΔU_{DC} can be determined as

$$\Delta U_{DC} = \sqrt{2 S_{out} \Delta f} = \Delta U_{JN} \sqrt{1 + \frac{U_{DC}}{U_{IM}} + \frac{U_{DC}}{U_{MN}}}, \tag{33}$$

where Δf is the frequency bandwidth of measurements and

$$\Delta U_{JN} = \sqrt{2 S(U_N) \Delta f} \tag{34}$$

is the voltage fluctuation caused by the low-frequency JN noise only. The minimum detected voltage can be estimated from the condition $\Delta U_{DC} = U_{DC}$.

The signal-to-noise ratio (SNR) of a STMD can be calculated as

$$SNR = \frac{U_{DC}}{\Delta U_{DC}} = \frac{P_{RF}}{P_{JN}} \sqrt{\frac{P_{MN}}{P_{MN} + P_{RF}}}, \tag{35}$$

where we intoduced the noise powers $P_{JN} = U_{JN} / \varepsilon_{res}$, $P_{MN} = U_{MN} / \varepsilon_{res}$ and took into account that $U_{IM} >> U_{JN}, U_{MN}$ for the typical STMD [19].

3.2 The performance of a STMD in the presence of thermal noise

The simple analysis of Eqs. (33), (35) demonstrates that there are two distinct regimes of operation of the resonance STMD in the presence of thermal noise. We shall classify them by the type of noise that limits the minimum detectable power of STMD $P_{\min}$ (power corresponding to $SNR = 1$).

The first regime corresponds to the case of relatively high frequencies of the input microwave signal, when $P_{MN} >> P_{RF}$ (for $P_{RF} \sim P_{\min}$). In this regime, similar to the conventional semiconductor diodes, the minimum detectable power is limited by the low-frequency JN noise, $P_{\min} = P_{JN}$, and the SNR of STMD is linearly proportional to the input microwave power P_{RF} ($SNR \propto P_{RF} / P_{JN}$).

The second regime takes place in the opposite limiting case of relatively low input frequencies, when $P_{MN} << P_{RF}$. In this case the SNR of the STMD increases with P_{RF} much slower than in conventional diodes, and is proportional to the square root of the input microwave power: $SNR \propto \sqrt{P_{RF} / P_{\min}}$. The minimum detectable power $P_{\min} = P_{JN}^2 / P_{MN}$ in this regime is limited by the magnetic noise in the FL of the MTJ.

The existence of two distinct regimes of STMD operation is illustrated in Fig. 2, where two curves calculated from Eq. (35) show the STMD SNR as functions of the input power for signal frequencies f_1 = 1 GHz (dashed blue line)

and f_2 = 25 GHz (red solid curve). It can be seen, that both curves (presented in logarithmic coordinates) demonstrate the clear change of slope from 1 to 1/2 in the region, where the input power P_{RF} is close to the characteristic power of the magnetic noise P_{MN} (which increases with the increase of the input signal frequency). The minimum detectable power $P_{\min}$ (corresponding to $SNR = 1$) in the high-frequency case is smaller than P_{MN} and lies in the region of the linear dependence of SNR on P_{RF} (solid red line in Fig. 2). The situation is opposite in the low frequency case (blue dashed curve in Fig. 2), when $P_{\min} > P_{MN}$ and lies in the region, where the slope of the SNR curve is equal to 1/2.

The evolution of the characteristic powers P_{MN} and $P_{\min}$ with the increase of frequency of the input microwave signal is shown in Fig. 3. The curve $P_{MN}(f)$ separates the plane into the region, where magnetic noise is dominant (above the curve), and the region, where the STMD operation is limited by the JN noise (below the curve). It is, clear, that the smallest detectable power is achieved near the border of these two regimes.

When an STMD based on an MTJ nanopillar is used as a sensor of microwave radiation, it is typically connected to a standard transmission line with the impedance of $Z_{TL} = 50\Omega$. The minimum detectable microwave power

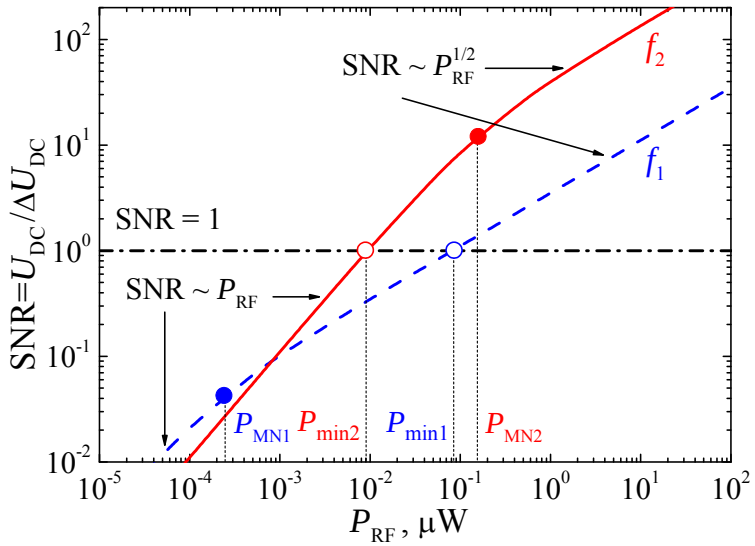

Fig. 2. Typical dependence of the SNR of STMD on the input microwave power P_{RF} calculated from Eq. (35) for two different frequencies of the input microwave signal: f_1 = 1 GHz (dashed blue line) and f_2 = 25 GHz (solid red line) [19]. $P_{\min}$ is the minimum detectable power of STMD (at SNR = 1) and P_{MN} is the frequency-dependent characteristic power of magnetic noise.

delivered to a 50-Ω transmission line can be written as [20]

$$P_{\min}[50\Omega] = \frac{1}{4}\frac{(R_0 + Z_{TL})^2}{Z_{TL} R_0} P_{\min} . \quad (36)$$

Using this expression and taking into account the size dependence of the STMD resistance ($R_0 \propto 1/r^2$), it is possible to show that $P_{\min}[50\Omega]$ has a clear minimum as a function of the nanopillar radius r. For instance, the optimum value of the nanopillar radius is $r_{opt} \approx 100$ nm for the input frequency $f = 5$ GHz (see the inset in Fig. 3).

As one can see from Fig.'s 2, and 3, the STMD operating in IP-regime has the performance comparable to the performance of conventional Schottky diode. Taking this into account we believe that such STMDs might be useful for developing practical devices involving microwave detectors, sensor systems, frequency analyzers, etc.

4 Large-angle out-of-plane dynamical regime of STMD operation

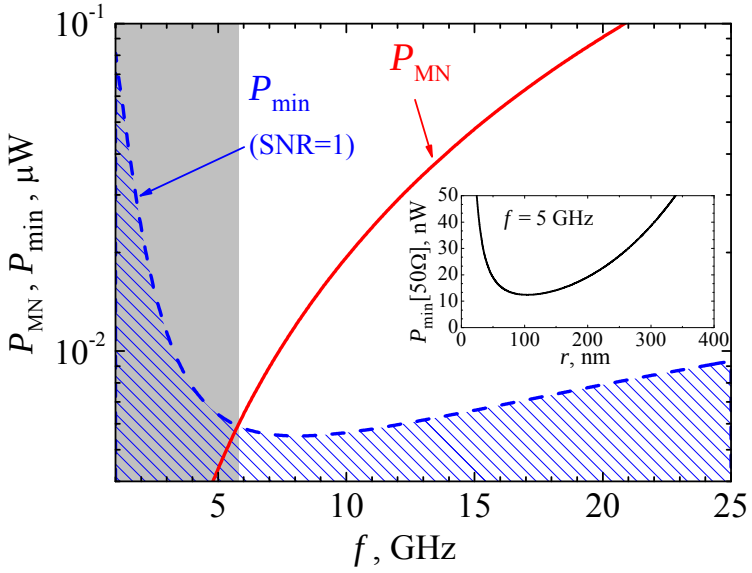

Fig. 3. The characteristic power of magnetic noise P_{MN} (solid red line) and minimum detectable power $P_{\min}$ of STMD (dashed blue line) as functions of the input microwave frequency f. The blue dashed area corresponds to undetectable signals ($P_{RF} < P_{\min}$) and gray shaded area shows the low-frequency STMD regime, where the magnetic noise is dominant in the whole practical region $P_{RF} > P_{\min}$. Inset: minimum detectible microwave power delivered to a 50-Ω transmission line $P_{\min}[50\ \Omega]$ for $f = 5$ GHz as a function of the radius r of the MTJ nanopillar.

In contrast to the well-known IP-regime of STMD operation, here we consider a different regime of operation of an STMD, based on the excitation of large-angle out-of-plane (OOP) magnetization precession under the action of an input microwave current $I_{RF}(t)$. We show that this regime of STMD operation is realized, when the STMD is biased by the perpendicular magnetic field $\mathbf{B}_0 = \mathbf{z}B_0$, which is smaller than the saturation magnetic field of the FL , i.e., $B_0 < \mu_0 M_s$ (μ_0 is the vacuum permeability).

4.1 Analytical description of OOP-regime

We consider a simple model of an STMD, formed by a circular MTJ nano-pillar (see Fig. 1). The magnetization of the pinned layer (PL) of the MTJ is assumed to be completely fixed and lie in the plane of the layer. The direction of the PL magnetization $\mathbf{p} = \mathbf{x}$ determines the spin-polarization axis. The radius r of the MTJ nano-pillar is assumed to be sufficiently small, so that the magnetization of the free layer (FL) $\mathbf{M} \equiv \mathbf{M}(t)$ is spatially-uniform and can be treated in the macrospin approximation. For simplicity, we neglect any in-plane anisotropy of the FL.

The dynamics of the unit magnetization vector $\mathbf{m}(t) = \mathbf{M}(t) / M_s$ in the FL under the action of a microwave current $I_{\mathrm{RF}}(t) = I_{\mathrm{RF}} \sin(\omega_s t)$ is governed by the Landau-Lifshits-Gilbert-Slonczewski (LLGS) equation:

$$\frac{d\mathbf{m}}{dt} = \gamma\left[\mathbf{B}_{eff} \times \mathbf{m}\right] + \alpha\left[\mathbf{m} \times \frac{d\mathbf{m}}{dt}\right] + \sigma I_{\mathrm{RF}}(t)\left[\mathbf{m} \times \left[\mathbf{m} \times \mathbf{p}\right]\right], \qquad (37)$$

$\mathbf{B}_{eff} = (B_0 - \mu_0 M_z)\mathbf{z}$ is the effective magnetic field, M_z is the z-component of vector $\mathbf{M}$.

Using the spherical coordinate system for the magnetization vector $\mathbf{m} = \mathbf{x}\sin\theta\cos\varphi + \mathbf{y}\sin\theta\sin\varphi + \mathbf{z}\cos\theta$, one can obtain the equations for the polar θ and azimuthal φ angles:

$$\frac{d\theta}{dt} = -\alpha\omega_P \sin\theta - \sigma I_{\mathrm{RF}} \sin(\omega_s t)\cos\theta\cos\varphi, \qquad (38a)$$

$$\frac{d\varphi}{dt} = \omega_P + \sigma I_{\mathrm{RF}} \sin(\omega_s t)\csc\theta\sin\varphi. \qquad (38b)$$

Here $\omega_P \equiv \omega_P(\theta) = \omega_H - \omega_M \cos\theta$ is the frequency of magnetization precession in the OOP-regime, $\omega_H = \gamma B_0$, and $\omega_M = \gamma\mu_0 M_s$. For simplicity, we neglected in Eqs. (38), second-order non-conservative terms ($\propto \alpha^2$ and $\propto \alpha I_{RF}$), which have a negligible effect on the magnetization dynamics.

In the OOP precessional regime, the magnetization precesses around $\mathbf{z}$ axis

along an approximately circular orbit, $\theta \approx const$, $\varphi \approx \omega_s t + \psi$, where ψ is the phase shift between the magnetization precession and the driving current. To analyze the conditions, under which the OOP regime is possible, one can average Eqs. (38) over the period of precession $2\pi/\omega_s$ and obtain the following equations for the slow variables θ and ψ:

$$\left\langle \frac{d\theta}{dt} \right\rangle = -\alpha\omega_P \sin\theta + v(a)\frac{\sigma_\perp I_{RF}}{2}\cos\theta\sin\psi\,, \qquad (39a)$$

$$\left\langle \frac{d\psi}{dt} \right\rangle = \omega_P - \omega_s + u(a)\frac{\sigma_\perp I_{RF}}{2}\frac{1}{\sin\theta}\cos\psi\,. \qquad (39b)$$

Here $a = P^2\sin\theta$ and

$$v(a) = \frac{1}{\sqrt{1-a^2}}\left[1 + \left(\frac{\sqrt{1-a^2}-1}{a}\right)^2\right], \qquad (40)$$

$$u(a) = \frac{1}{\sqrt{1-a^2}}\left[1 - \left(\frac{\sqrt{1-a^2}-1}{a}\right)^2\right]. \qquad (41)$$

Note, that for typical spin-polarization values $P \le 0.7$ both dimensionless functions $u(a)$ and $v(a)$ are very close to 1 for all angles θ.

The OOP regime of magnetization precession corresponds to a stationary solution of Eqs. (39) $\theta = \theta_s = const$, $\psi = \psi_s = const$. Solving Eqs. (39) in this case one can find the stationary value of the phase shift ψ_s:

$$\sin\psi_s = 2\frac{\alpha}{v}\frac{\omega_P}{\sigma_\perp I_{RF}}\tan\theta_s\,,\ \cos\psi_s = 2\frac{1}{u}\frac{\omega_s-\omega_P}{\sigma_\perp I_{RF}}\sin\theta_s\,. \qquad (42)$$

Eliminating ψ_s from the above equations, one obtains the characteristic equation for θ_s:

$$(\omega_s-\omega_P)^2\sin^2\theta_s + \frac{\alpha^2u^2}{v^2}\omega_P^2\tan^2\theta_s = \frac{u^2}{4}\sigma_\perp^2 I_{RF}^2\,. \qquad (43)$$

This equation for θ_s is a nonlinear equation, which, in a general case, can be only solved numerically.

One can see that Eq. (43) has solutions only for RF currents I_{RF} larger than a certain critical current I_{th}. At the threshold, $\omega_P(\theta_s) \approx \omega_s$, which allows one to obtain approximate expression for the threshold precession angle

$$\theta_{th} \approx \frac{\pi}{2} - \frac{\omega_H - \omega_s}{\omega_M} \qquad (44)$$

and determine the threshold microwave current $I_{th}(\omega_s)$ needed for the excitation of the OOP precession:

$$I_{th}(\omega_s) = 2\frac{\alpha}{\nu}\frac{\omega_M}{\sigma_\perp}\frac{\omega_s}{\omega_H - \omega_s}. \quad (45)$$

In the last expression we used the approximation $\sin(\theta_{th}) \approx 1$, which is valid for moderate magnetic fields and frequencies $\omega_H, \omega_s << \omega_M$.

One can show from Eqs. (39) that the OOP-regime will be stable if the following approximate conditions are fulfilled:

$$0 < \cos\theta_s < \frac{\omega_H}{\omega_M}, \quad \omega_s < \omega_H. \quad (46)$$

The first condition given by Eq. (46) means that the precession angle θ_s must be sufficiently large, because $\omega_H << \omega_M$ (we consider the case of a weak DC magnetic field) and $\cos\theta_s << 1$. The condition Eq. (46) restricts the region of existence of the OOP-regime to sufficiently low driving frequencies, determined by the bias magnetic field B_0.

The output STMD voltage in the OOP-regime can be found as

$$U_{DC} = I_{RF}\left\langle R(\beta)\sin(\omega_s t)\right\rangle = w(a) I_{RF} R_\perp \sin\psi_s, \quad (47)$$

where

$$w(a) = \frac{1}{\sqrt{1-a^2}}\left(\frac{1-\sqrt{1-a^2}}{a}\right). \quad (48)$$

Using Eq. (42) for $\sin\psi_s$ allows one to get the DC voltage as a function of θ_s only:

$$U_{DC} = 2\alpha\frac{w}{\nu}\frac{\omega_P}{\sigma_\perp} R_\perp \tan\theta_s. \quad (49)$$

This equation for U_{DC} can be simplified further by using the approximation $\sin\theta_s \approx 1$, $\cos\theta_s \approx \cos\theta_{th} \approx (\omega_H - \omega_s)/\omega_M$, valid for not very large driving currents:

$$U_{DC} \approx 2\alpha\frac{w}{\nu}\frac{\omega_M}{\sigma_\perp} R_\perp \frac{\omega_s}{\omega_H - \omega_s}. \quad (50)$$

Comparing Eq. (50) with Eq. (45) for threshold current $I_{th}(\omega_s)$, one can re-write the output DC voltage of the STMD as the function of threshold current $I_{th}(\omega_s)$:

$$U_{DC} \approx w I_{th}(\omega_s) R_\perp. \quad (51)$$

It follows from Eqs. (50), (51) that the output DC voltage of the STMD practically does not depend on the amplitude of RF current, provided that it is larger than the threshold current I_{th}.

4.2 Performance of a STMD in OOP-regime

Below we shall analyze an analytical solution for the STMD in the OOP-regime of operation, compare this solution with the results of numerical calculations and then also compare the performance of the STMD in IP- and OOP-regimes.

We shall consider the case of the STMD with the following typical parameters (see e.g. [13, 16]): radius of the STMD FL $r = 50$ nm, thickness of the STMD FL $d = 1$ nm, spin-polarization efficiency of current $P = 0.7$, resistance of STMD in perpendicular magnetic state ($\beta = \pi / 2$) $R_\perp = RA/(\pi r^2) = 1$ kΩ (giving resistance-area product of MTJ $RA = 7.854\ \Omega \cdot \mu\text{m}^2$), Gilbert damping constant $\alpha = 0.01$, saturation magnetization of the FL $\mu_0 M_s = 800$ mT.

We choose the magnitude of the external out-of-plane DC magnetic field as $B_0 = 200$ mT for the STMD in OOP-regime, which corresponds to the maximum OOP frequency $\omega_H = 2\pi \times 5.6$ GHz.

In the IP-regime of operation, the STMD will be characterized by the equilibrium angle $\beta_0 = \pi / 2$ between the equilibrium magnetization of the FL and the magnetization of the PL. Hence the equilibrium resistance of the STMD in the IP-regime is $R_0 = R_\perp = 1$ kΩ. We choose the magnitude of the external DC in-plane magnetic field as $B_0 = 14.1$ mT for the STMD in the IP-regime, that in accordance with the expression for FMR frequency $f_0 = \omega_0 / 2\pi = (\gamma / 2\pi)\sqrt{B_0(B_0 + \mu_0 M_s)}$, gives $f_0 = 3$ GHz. The resonance STMD sensitivity in the passive regime for such parameters is $\varepsilon_{res} \approx 2700$ V/W (see e.g. [17]), which is greater or comparable to the sensitivity of a typical unbiased Schottky diode [13].

We use Eq. (7) for the calculation of the output DC voltage of an STMD in the IP-regime as a function of the input microwave current magnitude I_{RF} and frequency $f = f_s = \omega_s / 2\pi$. These curves are indicated below in Figs. 4 and 5 by red dashed lines.

In order to verify the conclusions of the analytical theory of an STMD in the OOP-regime we numerically solved the LLGS Eq. (37) and then numerically calculated the output DC voltage of the detector as $U_{DC} = \langle I_{RF}(t) R(\beta) \rangle$. The results of our calculations are presented in Figs. 4, 5. Here solid blue lines and red dashed lines present the analytical dependencies of U_{DC} in the OOP- and IP-regimes (see Eq. (51) and Eq. (7)), respectively. Dots are the results of our numerical calculations. Black crosses and green circles correspond to the cases of

increasing and decreasing of the parameter (frequency ω_s or magnitude I_{RF} of the RF current), respectively. As one can see, the results of analytical theory are in reasonable agreement with the results of our numerical calculations.

As one can see from Fig. 4, in the OOP-regime the STMD works as a broadband low-frequency non-resonant microwave detector in contrast to the traditional resonance IP-regime. The response of the STMD to an input microwave current with magnitude I_{RF} is also substantially different in the cases of OOP- and IP-regimes of operation of an STMD (see Fig. 5). In the IP-regime, the output DC voltage U_{DC} of the detector is proportional to the input microwave power $P_{RF} = (1/2) I_{RF}^2 R_0$ (red dashed curve in Fig. 5, see also Eq. (7)). In contrast, the output DC voltage U_{DC} of the detector in the OOP-regime has a step-like dependence (blue solid curve and points in Fig. 5): $U_{DC} \approx 0$ for $I_{RF} < I_{th}(\omega_s)$ and $U_{DC} \approx const$ for $I_{RF} > I_{th}(\omega_s)$. Thus, in the OOP-regime, the STMD operates as a non-resonant broadband threshold microwave detector of low frequency RF signals.

It is important to note, that the results of our numerical simulations show the

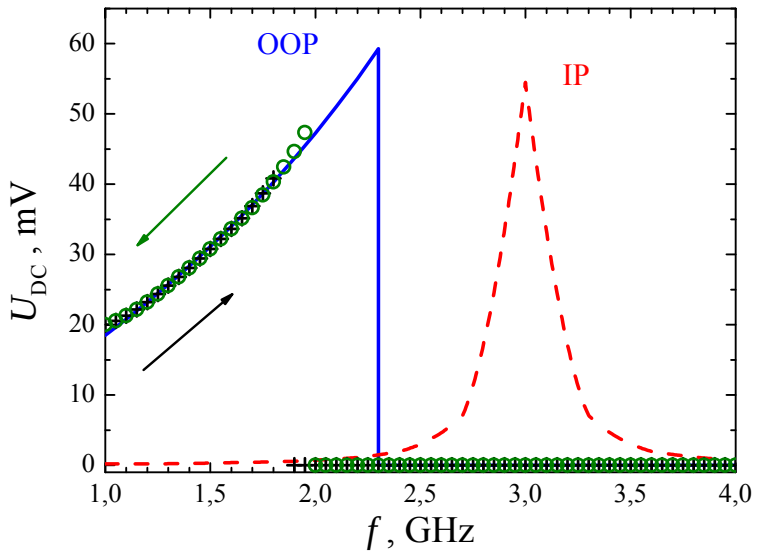

Fig. 4. Typical dependence of the output DC voltage U_{DC} of a STMD on frequency of input RF signal f in OOP- (solid line and points) and IP-regime (dashed line), respectively. Blue solid line is the analytical dependence given by Eq. (51), red dashed line is the analytical dependence given by Eq. (7). Points are the results of numerical simulations. Black crosses and green circles corresponded to the case when frequency is increased and decreased, respectively. I_{RF} = 0.2 mA.

existence of a hysteresis in the curves $U_{\mathrm{DC}}(f_s)$ and $U_{\mathrm{DC}}(I_{RF})$ in the OOP-regime (see Figs. 3, 4). The origin of this hysteresis lies in the "hard", or subcritical, scenario of excitation of the OOP precession: the precession angle θ_{th} that corresponds to the threshold current I_{th} does not coincide with the equilibrium magnetization angle and, therefore, for currents close to the threshold one the OOP regime may or may not be realized, depending on the history of the system. In experiments, the hysteresis may be "blurred" or may not be visible at all due to the influence of thermal fluctuations and other noises existing in real systems.

The results presented above correspond to the case of no DC bias current applied to the MTJ ($I_{\mathrm{DC}} = 0$). If this is not the case and $I_{\mathrm{DC}} \neq 0$, this current will partly compensate the damping in the FL MTJ, thus decreasing the threshold current $I_{th}(\omega_s)$. On the other hand, the in-plane anisotropy and/or the in-plane bias field in the FL may create an energy barrier between the regions of small-angle IP- and large-angle OOP-trajectories, which may result in increase of I_{RF}.

We also suggest that the OOP-regime of operation of a STMD might be responsible for an extremely large diode volt-watt sensitivity $\varepsilon \sim 10^5$ V/W

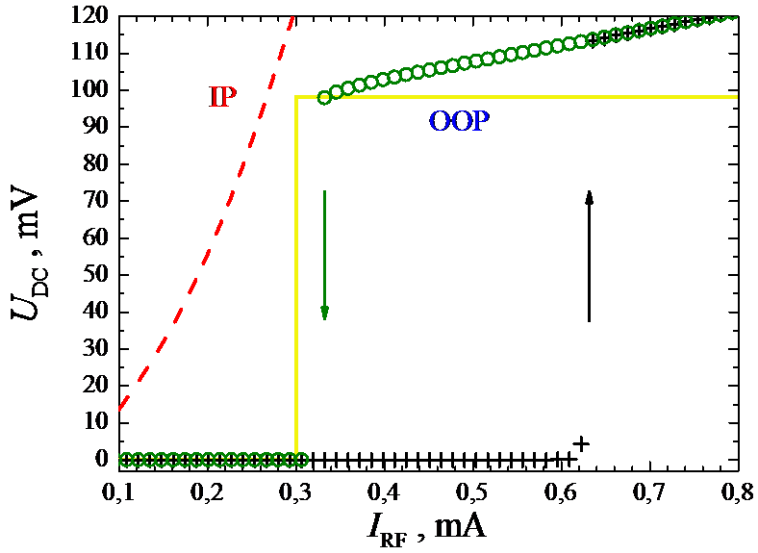

Fig. 5. Typical dependence of the output DC voltage U_{DC} of a STMD on input microwave current I_{RF} in OOP- (solid line and points) and IP-regime (dashed line), respectively. Blue solid line is the analytical dependence given by Eq. (51), red dashed line is the analytical dependence given by Eq. (7). Points are the results of numerical simulations. Black crosses and green circles corresponded to the case when the current is increased and decreased, respectively. $f = 3$ GHz.

observed in recent experiments with thermally-activated "non-adiabatic stochastic resonance" [21].

The STMD in the OOP-regime could be used as a base element for new energy harvesting devices, inasmuch as it has no resonance frequency, and, therefore, could accumulate energy from all the low-frequency region ($\omega_s < \omega_H$) of the microwave spectrum.

The energy conversion rate ζ of an STMD in the OOP-regime may be estimated as

$$\zeta = \frac{P_{DC}}{P_{RF}} \approx \frac{1}{2}\left(\frac{I_{th}(\omega_s)}{I_{RF}}\right)^2 \left(\frac{w}{w_0}\right)^2 , \qquad (52)$$

where P_{DC} is the output DC power of an STMD under the action of input microwave power P_{RF}, $w_0 \equiv w_0(a_s) = (1-a_s^2)^{-1/2}$, $a_s \approx P^2$. The maximum possible conversion rate $\zeta_{max} \approx 0.5w^2 / w_0^2 \approx 3.5\,\%$ is reached in the case $I_{RF} = I_{th}(\omega_s)$. We believe that this ratio is sufficiently large for practical applications in microwave energy harvesting.

5 Summary

In conclusion, we have demonstrated that there are two distinct regimes of STMD operation. One of them is characterized by a small-angle in-plane magnetization precession (IP-regime), while the other is characterized by a large-angle out-of-plane magnetization precession (OOP-regime). The performance of a STMD in these regimes is substantially different. In IP-regime STMD in the presence of noise can operate in two distinct sub-regimes, one of which is limited by magnetic noise and is different from the regime of operation of traditional semiconductor detectors. The developed formalism for STMD operating in IP-regime can be used for the optimization of noise-handling parameters of a STMD. We also has been demonstrated that there is a novel regime of operation of an STMD, based on the excitation of large-angle out-of-plane (OOP) magnetization precession. In this regime STMD operates as threshold detector of low-frequency RF signals. We believe that the OOP regime of STMD operation can be used for the development of novel types of threshold microwave detectors and might be responsible for extremely large diode volt-watt sensitivity observed in recent experiments with "non-adiabatic stochastic resonance" [21]. This regime of operation of an STMD might also be useful for the creation of energy harvesting devices based on STMD.

This work was supported in part by the Contract from the U.S. Army TARDEC, RDECOM*, by the grants ECCS-1001815 and DMR-1015175 from the National Science Foundation of the USA, by the grant from DARPA, by the Grant No. M/212-2011 from the State Agency of Science, Innovations and Informatization of Ukraine, and by the Grant No. UU34/008 from the State Fund

for Fundamental Research of Ukraine.

Disclaimer: Reference herein to any specific commercial company, product, process, or service by trade name, trademark, manufacturer, or otherwise, does not necessarily constitute or imply its endorsement, recommendation, or favoring by the United States Government or the Department of the Army (DoA). The opinions of the authors expressed herein do not necessarily state or reflect those of the United States Government or the DoA, and shall not be used for advertising or product endorsement purposes.

REFERENCES

1. J.C. Slonczewski, J. Mag. Mag. Mat. **159**, L1 (1996); J. Mag. Mag. Mat. **195**, L261 (1999).
2. L. Berger, Phys. Rev. B **54**, 9353 (1996).
3. J.A. Katine, F.J. Albert, R.A. Buhrman, E.B. Myers, and D.C. Ralph, Phys. Rev. Lett. **84**, 3149 (2000).
4. S. Urazhdin, N. O. Birge, W. P. Pratt, Jr., and J. Bass, Phys. Rev. Lett. **91**, 146803 (2003).
5. S.I. Kiselev, J.C. Sankey, I.N. Krivorotov, N.C. Emley, R.J. Schoelkopf, R.A. Buhrman, and D.C. Ralph, Nature (London) **425**, 308 (2003).
6. S. Kaka, M.R. Pufall, W. H. Rippard, T. J. Silva, S.E. Russek, and J.A. Katine, Nature (London) **437**, 389 (2005).
7. K. J. Lee, A. Deac, O. Redon, J.-P. Nozières, and B. Dieny, Nature Mater. **3**, 877 (2004).
8. I.N. Krivorotov, N.C. Emley, J.C. Sankey, S.I. Kiselev, D.C. Ralph, and R.A. Buhrman, Science **307**, 228 (2005).
9. F.B. Mancoff, N.D. Rizzo, B.N. Engel and S. Tehrani, Nature **437**, 393 (2005).
10. D. Houssameddine, U. Ebels, B. Delaët, B. Rodmacq, I. Firastrau, F. Ponthenier, M. Brunet, C. Thirion, J.-P. Michel, L. Prejbeanu-Buda, M.-C. Cyrille, O. Redon, and B. Dieny, Nature Mater. **6**, 447 (2007).
11. A. Ruotolo, V. Cros, B. Georges, A. Dussaux, J. Grollier, C. Deranlot, R. Guillemet, K. Bouzehouane, S. Fusil and A. Fert, Nature Nanotech. **4**, 528 (2009).
12. A.A. Tulapurkar, Y. Suzuki, A. Fukushima, H. Kubota, H. Maehara, K. Tsunekawa, D. D. Djayaprawira, N.Watanabe, and S. Yuasa, Nature **438**, 339 (2005).
13. S. Ishibashi, T. Seki, T. Nozaki, H. Kubota, S. Yakata, A. Fukushima, S. Yuasa, H. Maehara, K. Tsunekawa, D.D. Djayaprawira, and Y. Suzuki1, Appl. Phys. Express **3**, 073001 (2010).
14. A. Slavin, and V. Tiberkevich, IEEE Trans. Magn. **45**, 1875 (2009).
15. J.C. Sankey, Y. Cui, J.Z. Sun, J.C. Slonczewski, R.A. Buhrman, and D.C. Ralph, Nat. Phys. **4**, 67 (2008).
16. C. Wang, Y.-T. Cui, J.Z. Sun, J.A. Katine, R.A. Buhrman, and D.C. Ralph, Phys. Rev. B **79**, 224416 (2009).
17. C. Wang, Y.-T. Cui, J.Z. Sun, J.A. Katine, R.A. Buhrman, and D.C. Ralph, J. Appl.

Phys. **106**, 053905 (2009).
18. N.B. Lukyanchikova, *Noise research in semiconductor physics*, (CRC Press, Amsterdam, 1996).
19. O. Prokopenko, G. Melkov, E. Bankowski, T. Meitzler, V. Tiberkevich, and A. Slavin, Appl. Phys. Lett. **99**, 032507 (2011).
20. D.M. Pozar, *Microwave Engineering, 3rd ed.* (Wiley, New York, 2005).
21. X. Cheng, C.T. Boone, J. Zhu, and I.N. Krivorotov, Phys. Rev. Lett. **105**, 047202 (2010).